GNSS Autonomous Integrity Monitoring with Barometric Pressure Measurements and Weather Data

Maximilian Simonetti and Omar García Crespillo
Institute of Communications and Navigation, German Aerospace Center (DLR)

BIOGRAPHY

Maximilian Simonetti received his Master's in Aerospace Engineering from the Technical University of Munich in 2021 and his Bachelor's in Aerospace Engineering from Sapienza University of Rome in 2018. He is currently a scientific employee of the Navigation Department of the German Aerospace Center (DLR), where he works within the Integrated Navigation Systems Integrity group. His field of research includes multi-sensor navigation architectures for aviation and UAVs.

Omar García Crespillo is the leader of the Integrated Navigation Systems Integrity group at the Navigation department of the German Aerospace Center (DLR). He holds a P.hD. from the Swiss Federal Institute of Technology (EPFL), 2022 and a M.Sc. in Telecommunication Engineering from the University of Malaga in Spain, 2013. His current field of research includes ARAIM and integrity monitoring in GNSS/INS and high accuracy GNSS for safe ground and air transportation systems.

ABSTRACT

Vertical navigation is essential for new aviation operations like precision approaches and automatic landing which are expected to be primarily based on Global Navigation Satellite Systems (GNSS). However, achieving tighter vertical requirements with GNSS is challenging due to the inherent geometrical limitations. Current Aircraft-Based Augmentation Systems (ABAS) developments focus on proving that Advanced Receiver Autonomous Integrity Monitoring (ARAIM) is able to provide a robust operation for horizontal services and vertical guidance via the use of Multi-frequency and Multi-constellation GNSS. Although ARAIM can achieve high levels of integrity, the availability and continuity of the system may be compromised by the loss of satellites or high presence of cycle slips. For this reason, the support of onboard sensors like barometers is essential to guarantee all the vertical navigation requirements and extend the achievable accuracy and integrity for future even more stringent operations. This paper aims at augmenting GNSS navigation with geodetic altitude obtained from aircraft barometric pressure measurements and external weather data within a robust navigation architecture based on ARAIM. The present work describes the derivations of the threat and error models that are required for the inclusion of this barometric geodetic altitude into ARAIM. The improvement in availability is simulated world-wide with respect to the expected uncertainty of the geodetic barometric altitude. Then, real flight data is used to show the benefit of the barometer augmentation on the integrity of the navigation solution under real operational scenarios. The error models are obtained from several hours of flight data collected during a flight tests campaign performed in 2018 with the German Aerospace Center's (DLR) Dassault Falcon aircraft.

I. INTRODUCTION

Vertical navigation is essential for safe Air Traffic Management (ATM) and, in particular, it is crucial for aircraft vertical separation. This is ensured traditionally by the concept of flight levels (FL), that are surfaces of constant standard pressure altitude (SKYbrary, 2021). This altitude information is obtained from pressure measurements performed by barometers within airborne Air Data Systems (ADS) when setting the International Standard Atmosphere (ISA) Mean Sea Level isobar (MSL) as reference. Because of several reasons as, among others, differences in altitude scales and reference, this altitude information can differ by up to hundreds of meters from the true geodetic altitude, that is the geometric altitude above the reference ellipsoidal surface of the Earth (e.g., WGS84).

In aviation, pressure altitude is not actually converted to geodetic altitude, but, in certain flight phases, the standard pressure altitude undergoes some transformations. Below so-called transition altitudes indeed, altitude information for aircraft separation is not the only one required and reliable information about separation from to the ground is needed too. This has been traditionally achieved with barometers by setting as the reference isobar in the pressure altitude computation the isobar at the airport's location (QFE approach) or an estimate of the actual MSL isobar (QNH approach) at the same horizontal location of the airport (RTCA, 2020). Further pressure altitude corrections in aviation also try to account for differences between the real atmospheric temperature behavior and its model that is used in the pressure altitude equation (ICAO, 2006b). However, depending on the actual altitude and distance from the airport, pressure altitude can still remarkably deviate from the actual geometric altitude above MSL (for QNH) or above the airport (for QFE). This means that these corrected pressure altitudes will

still remarkably differ from the actual geodetic altitude too, once their references are shifted to the reference ellipsoid of the Earth.

Vertical navigation based on accurate geodetic altitude instead is essential for different applications. First, it is crucial for new aviation operations like precision approaches and automatic landing (ICAO, 2013) which are foreseen to be mainly relying on GNSS. However, the compliance of GNSS-based navigation with tighter vertical requirements is demanding due to the inherent GNSS geometrical limitations and external interferences. The augmentation with onboard sensors could help increase accuracy and safety. This falls under the definition of ABAS and, in particular, of Aircraft Autonomous Integrity Monitoring (AAIM) (Garcia Crespillo, 2022). The strength of such systems is that they do not rely on infrastructures external to the aircraft, as opposed to Satellite-based Augmentation System (SBAS) or Ground-based Augmentation Systems (GBAS), which rely on GNSS corrections transmitted from geostationary satellites or from ground stations, respectively. An additional use case requiring safe geodetic altitude information consists in new Urban Air Mobility (UAM) applications, which are foreseen to run closer to the ground and will require robust geodetic altitude determination for guidance, navigation, collision avoidance and air traffic management (Torens et al., 2021).

The development of ABAS systems is focused on proving that ARAIM can robustly sustain operations for horizontal services and vertical guidance thanks to the use of Multi-constellation and Multi-frequency GNSS. Even though ARAIM can ensure high levels of integrity, the attainable protection levels (PL) are limited by the overbounding of error distributions to account for worst-case expected performances. Moreover, due to the required maneuvers in terminal vicinity and precision procedures, the availability and continuity of the system may be jeopardized by the loss of satellites while banking or by the presence of cycle slips (Garcia Crespillo, 2022).

The use of onboard sensors like barometers can support GNSS-based positioning to guarantee the vertical navigation requirements and to extend the achievable accuracy and integrity of future stringent operations. However, the use of barometers in combination with GNSS for geodetic altitude navigation presents different challenges and requires the following aspects:

1. Rigorous conversion from pressure altitude to geodetic altitude.

2. Error models of the resulting geodetic altitude.

3. Dedicated sensor failure analyses needed for the integrity monitoring.

Previous work regarding the conversion of barometric pressure to altitude and the augmentation of GNSS-based systems with barometers is found in literature. Gaglione et al. (2015) consider the differences between standard pressure and geodetic altitudes in regard to their references but not to their scales. S. Jan et al. (2008) and (Lee et al., 2016) do the same but, additionally, correct the pressure altitude by using limited external weather data. Finally, in (Xu et al., 2021), no conversion from barometric pressure to geodetic altitude is mentioned. Therefore, in none of the aforementioned previous work, pressure altitude is at the same time corrected with weather data and rigorously converted to geodetic altitude. Furthermore, the test scenarios themselves of this previous work limit a comprehensive analysis of pressure altitude and its augmentation capabilities when applied to aircraft navigation. Indeed, the methodologies of Gaglione et al. (2015) and Lee et al. (2016) are applied to series of measurements performed while the sensors were kept at constant altitudes that are much smaller than typical aviation altitudes. The findings of S. Jan et al. (2008), instead, are based on pressure altitudes computed exclusively from meteorological observation data, in the sense that both the "measured" and the reference pressures are the result of historical weather observation. The analyses of Xu et al. (2021) are based on an aircraft flight simulation and on real data collected with a car. The error model derived by Lee et al. (2016) is applied to a simulation too, and in particular of an Unmanned Aerial Vehicle (UAV) flight approach.

In summary, none of the aforementioned test scenarios allows to properly evaluate the effects on actual pressure measurements caused by altitude variations, flight dynamics, and weather phenomena, such as wind.

The present work aims at augmenting GNSS navigation with geodetic altitude obtained from aircraft barometric pressure measurements and external weather data within a robust navigation architecture based on ARAIM. A detailed description of the methodology for computing this geodetic altitude is given by the authors in (Simonetti and Garcia Crespillo, 2021). The paper is organized as follows. Section II extends the ARAIM baseline algorithm to consider additional barometric geodetic altitude measurements. Moreover, it presents the derivation of the nominal error models and of the threat model that are necessary for this inclusion. Section III presents world-wide availability simulations results of the proposed navigation architecture for different uncertainties of the geodetic baro measurements. The barometric augmented ARAIM algorithm is then evaluated with flight data in Section IV. Section V provides some closing remarks and aspects as well as future work.

II. MAIN ASPECTS OF THE BASELINE ARAIM ALGORITHM

Advance Receiver Autonomous Integrity Monitoring (ARAIM) is an augmentation system for GNSS which ensures the integrity of the positioning solution. This section summaries the most important aspects related to the baseline ARAIM algorithm which are relevant for this publication. For further details, the reader is referred to Working Group C (2016) and Blanch et al. (2015). At each epoch, all considered Galileo and GPS satellite measurements are used to compute a navigation solution $\mathbf{x}$, which

contains the receiver position and receiver clock biases. The position and clock unknowns are typically solved via linearization of the pseudorange observation equation and with iterations based on the following weighted least-squares estimator:

$$\Delta\hat{\mathbf{x}} = \mathbf{S}\Delta\mathbf{z} = \left(\mathbf{G}^T\mathbf{W}\mathbf{G}\right)^{-1}\mathbf{G}^T\mathbf{W}\Delta\mathbf{z}\,, \tag{1}$$

where $\Delta\mathbf{z}$ contains the vector of pseudorange measurements $\Delta\boldsymbol{\rho} = \boldsymbol{\rho} - \tilde{\boldsymbol{\rho}}$, after dual-frequency and tropospheric corrections and smoothing, minus the expected ranging values based on the estimated satellites and user's position. The geometry matrix $\mathbf{G}$ is:

$$\mathbf{G} = \begin{pmatrix} \mathbf{u}_{\text{Gal}}^1 & 1 & 0 \\ \vdots & \vdots & \vdots \\ \mathbf{u}_{\text{Gal}}^{n_{\text{Gal}}} & 1 & 0 \\ \mathbf{u}_{\text{GPS}}^1 & 0 & 1 \\ \vdots & \vdots & \vdots \\ \mathbf{u}_{\text{GPS}}^{n_{\text{GPS}}} & 0 & 1 \end{pmatrix}\,, \tag{2}$$

where n_{GPS} and n_{Gal} denote the number of available GPS and Galileo pseudorange measurements, respectively. The vector $\mathbf{u}^i$ denotes the line of sight vector, in the ENU frame, from the user to the ith satellite.

The estimator's weight matrix $\mathbf{W}$ is the inverse of the measurement covariance matrix $\mathbf{C}_{int}$ used for integrity:

$$\mathbf{C}_{int} = \text{diag}\left(\left[\sigma_{int,\text{Gal},1}^2 \quad \cdots \quad \sigma_{int,\text{Gal},n_{\text{Gal}}}^2 \quad \sigma_{int,\text{GPS},1}^2 \quad \cdots \quad \sigma_{int,\text{GPS},n_{\text{GPS}}}^2\right]\right)\,,$$

$$\text{with}\quad \sigma_{int,\text{Gal},i}^2 = \sigma_{URA,\text{Gal},i}^2 + \sigma_{\text{Gal},i}^2 \quad \text{and}\quad \sigma_{int,\text{GPS},i}^2 = \sigma_{URA,\text{GPS},i}^2 + \sigma_{\text{GPS},i}^2\,, \tag{3}$$

where $\sigma_{URA,i}$ denotes the i_{th} satellite's standard deviation of the clock and ephemeris error used for integrity. The second parameter σ_i is an additional term for residual tropospheric and user side errors (typically multipath and noise) (Working Group C, 2016).

Additionally, ARAIM is based on Multiple Hypothesis Solution Separation (MHSS) algorithm, where the GNSS faults that need to be monitored are based on the values of probabilities of the single satellite faults $P_{sat,\text{Gal}}$ and $P_{sat,\text{GPS}}$ and of the constellation-wide faults $P_{const,\text{Gal}}$ and $P_{const,\text{GPS}}$.

First, the algorithm computes the maximum number of concurrent faults that must be monitored. This is denoted with $N_{fault,max}$ and defined as:

$$N_{fault,max} = \max\{r \in 1, ..., N_{meas}|P_{multiple}\left(r+1, P_{event,1}, ..., P_{event,N_{meas}+N_{const}}\right) \leq P_{thres}\}\quad, \tag{4}$$

where P_{thres} is the chosen threshold for the integrity risk coming from unmonitored faults, $N_{meas} = n_{\text{GPS}} + n_{\text{Gal}}$ and N_{const} denotes the number of available GNSS constellations, which can be 1 or 2, since only GPS and Galileo are considered. Naturally, at a given epoch, $N_{const} = 0$ if no satellite measurement is available. In Equation 4, $P_{multiple}\left(r, P_{event,1}, ..., P_{event,N_{meas}+N_{const}}\right)$ denotes the probability of all the fault modes consisting of at least r independent events, with

$$P_{event,i} = P_{sat,i}$$
$$\text{with } i \in 1, ..., N_{meas} \quad \text{and}\quad j \in 1, ..., N_{const}\,. \tag{5}$$
$$P_{event,N_{meas}+j} = P_{const,j}$$

Secondly, all the $N_{subsets}$ possible combinations of $N_{fault,max}$ or less events are determined. All the satellite subsets that correspond to these combinations are then formed, i.e., the algorithm forms $N_{subsets}$ satellites subsets, where the kth subset contains all the satellites that are fault-free in the kth combination, with $k = 1...N_{subsets}$ (Blanch et al., 2015).

The ARAIM algorithm computes then for each of these combinations the corresponding k^{th} navigation solution that is obtained from the measurements of all the satellites in the kth subset. The navigation solutions computed based on these satellite subsets are known as fault-free solutions and are denoted with $\mathbf{x}^k$ (Working Group C, 2016).

Based on a comparison of the all-in-view and the fault-free solutions with a solution separation test, it is possible to determine whether a certain fault mode is present. In the case of no fault detection, it is possible to compute an horizontal and a vertical protection levels HPL and VPL.

In order to build the solution separation tests and to compute the protection levels, the error model and threat model is therefore important. Some of the relevant parameters are expected to be obtained from an Integrity Support Message (ISM):

- the nominal bias used for integrity $b_{nom,GPS}$, or $b_{nom,Gal}$,

- the standard deviation of the clock and ephmeris errors used for integrity σ_{URA},

- the standard deviation of the clock and ephemeris error used for accuracy and continuity, $\sigma_{URE,Gal}$, or $\sigma_{URE,GPS}$.

- The probability of satellite and constellation-wide fault P_{sat} and P_{const}

The standard deviations σ_{URA} and the nominal biases b_{nom} constitute the GNSS nominal error models for integrity. The GNSS nominal error models for accuracy and continuity consist of the standard deviations for accuracy and continuity σ_{URE}, instead. The protection levels are computed based on the following implicit equation (Blanch et al., 2015):

$$2Q\left(\frac{xPL - b_q^0}{\sigma_q^0}\right) + \sum_{k=1}^{N_{subsets}} p_{fault,k}Q\left(\frac{xPL - T_{k,q} - b_q^k}{\sigma_q^k}\right) = P_{HMI,mon,q} \qquad \text{with } q \in 1,2,3 \qquad (6)$$

where $p_{fault,k}$ is the prior probability of the kth fault mode, while $T_{k,q}$, σ_q^k, and b_q^k are the solution separation threshold, the nominal bias projected into the dimension q and the variance of the navigation solution in the dimension q, respectively, of the kth subset. The superscript 0 refers to the subset number 0, that corresponds to the all-in-view set of satellites.

The dimensions 1, 2 and 3 correspond to the East, North and Down spacial components, respectively. Depending on the dimension q, the term xPL represents the horizontal protection level along the East or North axis, or the vertical protection level, which are denoted by HPL_E, HPL_N and VPL, respectively. The overall horizontal protection level HPL is the square root of the sum of the squares of HPL_E and HPL_N. The term $P_{HMI,mon,q}$ corresponds to the faults probability that may result in Hazardously Misleading Information in the dimension q and that needs to be monitored. Finally, $Q(\cdot)$ is the tail probability function of a zero mean unit normal distribution.

The ARAIM algorithm requires the definition of some further constants and design parameters that are related to integrity, like P_{thres}, as well as others related to accuracy and continuity (Working Group C, 2016). Their description is out of the scope of the present paper, since the baro-augmentation has no influence on them. For the same reason, the values that were assigned to these constants and parameters within the implementation of the baro-augmented ARAIM (see Sections IV and V) are the ones that are used in (Walter and Blanch, 2019) or prescribed or recommended in (Working Group C, 2016) for LPV-200.

III. BARO-AUGMENTED ARAIM CONCEPT

In this work barometric measurements are combined with GNSS to improve the position solution and integrity of the system. In order to use barometric measurements to augment ARAIM, they are first translated into geodetic altitude. This process is presented in Figure 1. The conversion to barometric geodetic altitude from airborne pressure measurements by using weather information was previously introduced by the authors in (Simonetti and Garcia Crespillo, 2021).
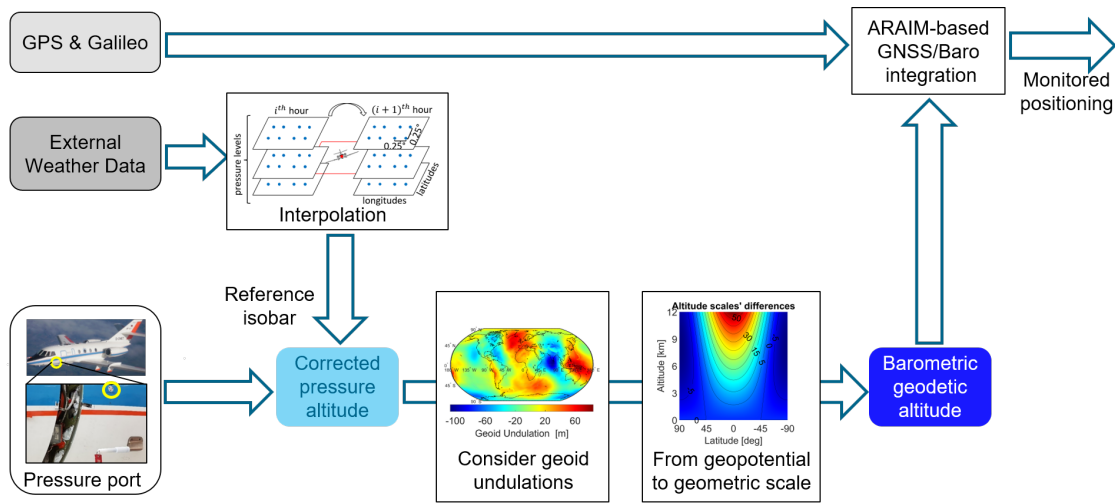

Figure 1: GNSS/barometer integration concept

The external weather data is in this work obtained from a publicly available external weather dataset, which contains data on a regular longitude-latitude grid at each UTC full hour. A four-dimensional interpolation is then applied to obtain pressure and temperature values along the flight trajectory. These values are then used as the pressure and temperature of the reference isobar in the pressure altitude equation. Because of the usage of external weather data, this corrected altitude is in (Simonetti and Garcia Crespillo, 2021) referred to as *weather-corrected pressure altitude*. For the sake of shortness, it is in this paper

called *corrected pressure altitude*. From this, the corresponding geodetic altitude, that the authors denominate here *barometric geodetic altitude*, is obtained through a two-steps conversion.

The main focus of the present paper is to describe the integration of this geodetic altitude with Galileo and GPS measurements. This integration is based on ARAIM, as shown in Figure 1, and is in this paper referred to as the *baro-augmentation*. Analogously, the resulting algorithm is herein called *baro-augmented ARAIM*.

The inclusion of the barometric measurements into the positioning least-squares and ARAIM is done by augmenting the vector $\Delta\mathbf{z}$ in Equation 1 by one element, that is the difference between the barometric geodetic altitude measurement and the estimated user's geodetic altitude:

$$\Delta\mathbf{z}_{baro\text{-}ARAIM} = \begin{bmatrix} \Delta\rho \\ h_{Baro} - \hat{h} \end{bmatrix}, \tag{7}$$

with the subscript *baro-ARAIM* featuring all the ARAIM parameters that are modified after the baro-augmentation.
As a result, the geometry matrix gets also augmented by one additional row, i.e.:

$$\mathbf{G}_{baro\text{-}ARAIM} = \begin{bmatrix} \mathbf{G} \\ \mathbf{G}_{Baro} \end{bmatrix} \quad, \text{ with } \quad \mathbf{G}_{Baro} = \begin{bmatrix} 0 & 0 & 1 & 0 & 0 \end{bmatrix}. \tag{8}$$

In a similar way to what is done for the GNSS measurements, the integration of the barometric geodetic altitude into ARAIM requires the definition of corresponding nominal error models and threat model.
After deriving the nominal error model for integrity, $\mathbf{C}_{int}$ can be then augmented as:

$$\mathbf{C}_{int,baro\text{-}ARAIM} = \begin{bmatrix} \mathbf{C}_{int} & \mathbf{0} \\ \mathbf{0} & \mathbf{C}_{int,Baro} \end{bmatrix} \quad, \text{ with } \quad \mathbf{C}_{int,Baro} = \sigma^2_{int,Baro}. \tag{9}$$

The threat model of the barometric geodetic altitude measurement consists in the probability of fault P_{baro} of the system that produces the barometric geodetic altitude measurements. After deriving this, the subsets determination described in Subsection II can be modified by simply extending Equation 5 with:

$$P_{event,N_{meas}+N_{const}+1} = P_{Baro}. \tag{10}$$

Figure 2 presents a visual summary of which are the required parameters for the baro-augmentation and where they play a role in the baro-augmented ARAIM algorithm.
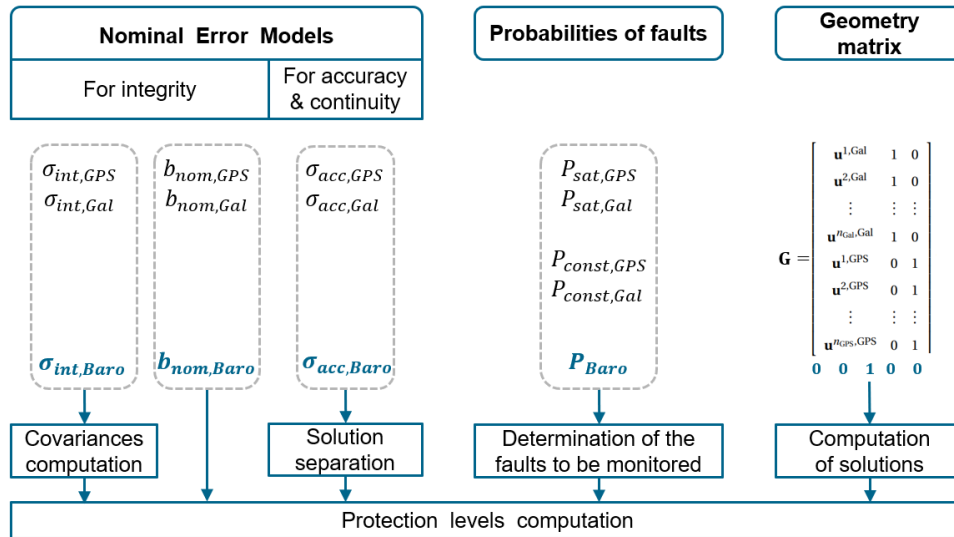

Figure 2: Key parameters in the baro-augmented ARAIM

The next subsections describe the adopted methodology for the derivation of such parameters.

1. Nominal Error Models

It is required that a nominal error models for integrity is an upper bound for all possible errors with the exception of 10^{-7} of the cases at most.

Suitable error models based on experimental flight data were derived in (Simonetti and Garcia Crespillo, 2021). This was obtained by deriving a Gaussian overbound of the residual weather corrected geodetic altitude over several flights in the Cumulative Density Function (CDF).

The value of the parameters found in Simonetti and Garcia Crespillo (2021) based on more than 20 hours of flight test are the following: $\sigma_{int,Baro} = 15$ m and $b_{nom,Baro} = 1.1$ m. This integrity model is used in this work as a starting point for the availability simulations and is then used in the real filght data evaluation. The same distribution which was employed for the derivation of the aforementioned model is also used for the determination of the nominal error model for accuracy and continuity. This is found with a zero-mean Gaussian distribution overbounding the 95% of the residual error as shown in Figure 3. The standard deviation of the nominal error model for accuracy and continuity was found to be $\sigma_{acc,Baro} = 4.465$ m.

The folded CDFs of the distributions corresponding to the derived nominal error models for integrity and accuracy are shown in Figure 3, along with the residual error distribution.
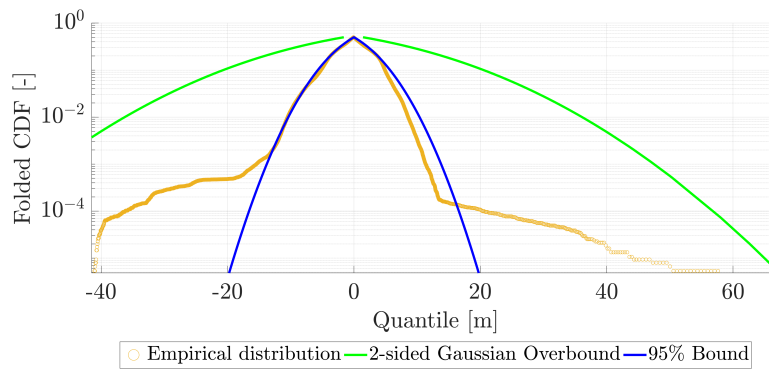

Figure 3: Nominal error models

2. Threat Model

The threat model consists in the probability of fault in the computation of the barometric geodetic altitude, P_{Baro}. This probability can be identified with the fault rate, in terms of cases per hour. The fault propagation to the geodetic altitude can be studied by a fault tree analysis. A fault in the geodetic altitude can be developed with two top-level branches, where one is related to the airborne pressure measuring performance and the other is related to the external data that is used for the pressure altitude correction, as shown in Figure 4.

Based on (Lerro and Battipede, 2021), the airborne side may be decomposed down to the hardware Air Data System (ADS) parts which are involved in the performance and analog-to-digital conversion of the static air pressure measurements. This concept focuses on an ADS designed for small aircraft transportation (SAT) use cases. The system is analyzed down to the heater, probe and piping of the Pitot tube, as well as down to the two hardware (HW) boards (one is redundant) and the pressure transducer that are part of the Air Data Computer (ADC). Lerro and Battipede (2021) obtain the fault rates (FR) from (Quanterion Solutions Incorporated, 2016), which provides statistics data for a plethora of components, including mechanical, electromechanical, and electronic assemblies. The fault rate in the top level of the airborne side can be then computed starting from the lowest levels, based on a bottom-up system safety assessment (SSA) approach. This leads to a fault rate of $6.91 \times 10^{-5} \mathrm{h}^{-1}$. The fault rates of all the involved systems and parts are shown in Figure 4, whereby the unit of measure, i.e. h^{-1}, is omitted.

Adopting this airborne FR for airplanes in the transport category, that is classified according to EASA CS-25 or FAA's 14 CFR Part 25, can be considered a conservative approach, since the ADS analyzed in (Lerro and Battipede, 2021) is designed for SAT, which belongs to EASA CS-23 (Lerro and Battipede, 2021; Piwek and Wiśniowski, 2016; Di Vito and Torrano, 2017). Indeed, it is expected that EASA CS-25 classified airplanes are equipped with ADSs of a higher grade with respect to the EASA CS-23 classified ones.

The baro-augmentation is expected to work in an operational scenario. For this reason, the external weather data used for the pressure altitude correction will need to be weather forecasts data. In the present work, the external weather data was obtained from the European Centre for Medium-range Weather Forecast (ECMWF). ECMWF does not provide any information that may
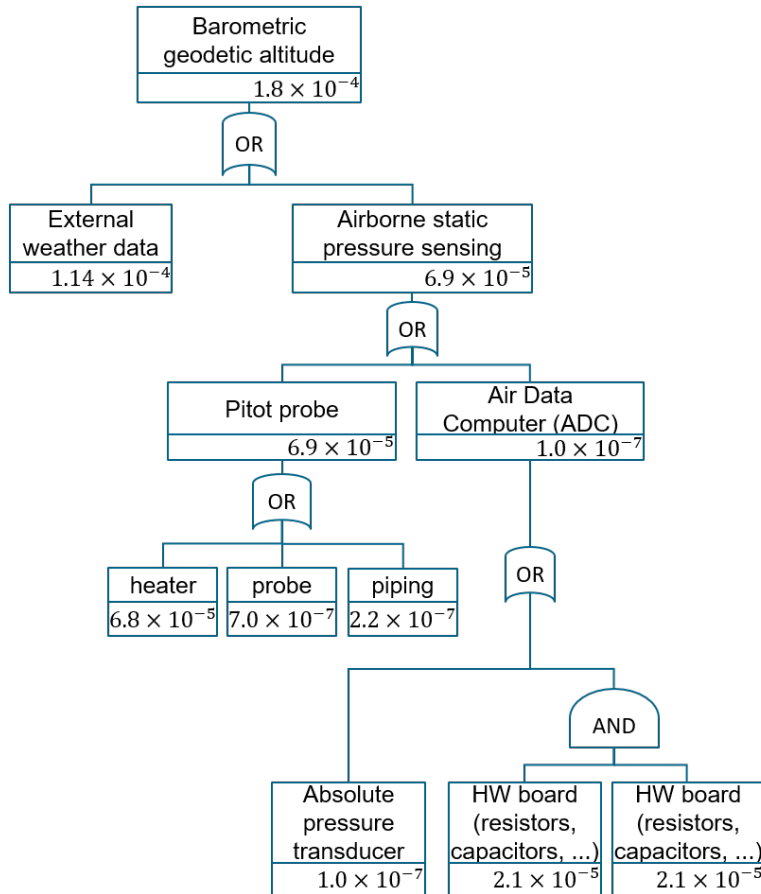
Figure 4: Fault tree (based on (Lerro and Battipede, 2021)) of the barometric geodetic altitude

be useful for estimating the FR in its weather forecasts. However, it makes available a list of documented, known, solved or unresolved issues in its global weather reanalysis dataset ERA5 (Hersbach et al., 2018). A weather reanalysis depicts past weather in the currently most complete way possible. It is a combination of measurements with past short-range weather forecasts, recomputed with the latest weather forecasting models (ECMWF, 2020). The ERA5 was started in 2016 and since 2017 always lags 2-3 months behind the present. This reanalyis was run backwards to 1959 too. Since 2019, ECMWF additionally makes available an ERA5 subset, known as ERA5T, that provides preliminary data for ERA on a daily basis, with only a 5-day delay with respect to the present. This is summarized by Figure 5.

This work considers the ERA5T dataset for deriving an estimate of the weather data FR, since the ERA5T is much closer to real-time when compared to the ERA5 dataset. ECMWF provides a list of the issues of the ERA5T as well. Based on this list, it is possible to count the issues that can be considered as weather data faults within the context of the weather-data pressure altitude correction.

The FR in the weather data may be computed from the number of weather data faults and the time-span covered by the weather data, based on the methodology described by Walter et al. (2019) for the determination of GNSS fault rates for ARAIM.

In the case of ERA5T, it was considered that none of the reported issues could potentially lead to a fault in the pressure altitude correction. However, the number of ERA5T faults was herein increased by 2, as suggested by Walter et al. (2019). This methodology returns a value of $1.14 \times 10^{-4} \mathrm{h}^{-1}$ for the weather data FR, when considering the time-span from the ERA5T release date to the 1st of June 2022, i.e. when the described analysis was performed.

Considering the airborne and the weather data sides of the fault tree, the value of the estimate FR in the barometric geodetic altitude is $1.83 \times 10^{-4} \mathrm{h}^{-1}$, as shown in the fault-tree's top level in Figure 4.
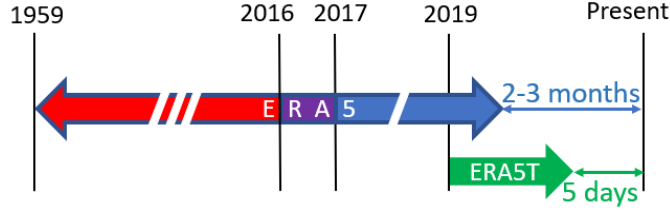
Figure 5: Overview of the ECMWF reanalysis weather datasets considered within this work

IV. AVAILABILITY SIMULATIONS

The performance of the baro-augmentation is first assessed by including it into the MATLAB® algorithm availability simulation tool (MAAST) (Walter and Blanch, 2019). This toolset simulates Galileo and GPS constellations over a given time length T and runs at every epoch, with a given time step Δt, the ARAIM algorithm on all the grid points of a global latitude-longitude grid with given latitude and longitude steps ΔL and $\Delta \lambda$, respectively. The values used for the simulation are: $T = 86400$ s, $\Delta T = 300$ s, $\Delta L = 10$ deg. and $\Delta \lambda = 10$ deg. The criteria for the availability determination, compatible with LPV-200 requirements, are the following: $HPL \leq HAL = 40$ m, $VPL \leq VAL = 35$ m, $EMT \leq 15$ m and $\sigma_{v,acc} \leq 1.87$ m, where HAL and VAL stand for Horizontal and Vertical Alert Limit, respectively. EMT stands for Effective Monitoring Threshold, while $\sigma_{v,acc}$ denotes the standard deviation of the vertical position solution. Both of these quantities are defined in (Blanch et al., 2015). The following values are also used for the GNSS parameters that are needed for ARAIM, based on (Working Group C, 2016):

- $\sigma_{URA,GPS,i} = 1$ m, $\quad \sigma_{URE,GPS,i} = 2/3$ m, $\quad b_{nom,GPS,i} = 0.75$ m $\quad P_{sat,i} = 10^{-5}$ $\quad$ for $i = 1...n_{GPS}$,

- $\sigma_{URA,Gal,i} = 1$ m, $\quad \sigma_{URE,Gal,i} = 2/3$ m, $\quad b_{nom,Gal,i} = 0.75$ m $\quad P_{sat,i} = 10^{-5}$ $\quad$ for $i = 1...n_{Gal}$,

- $P_{const,GPS} = 10^{-8}$h^{-1}, $\quad P_{const,Gal} = 10^{-4}$h^{-1} .

Finally, the satellite elevation mask angle is 5 deg.

As explained in Subsection II, ARAIM requires the definition of some further constants and design parameters that are related to integrity, accuracy and continuity. The default values assigned to these additional parameters for vertical ARAIM in (Walter and Blanch, 2019) were kept here too. The nominal error models in Section III.1 are used for the simulations presented in Subsection IV.2. Subsection IV.1 performs first a sensitivity analysis of the availability with respect to other possible error model parameters.

1. Study on the Availability Sensitivity to Variations in the Nominal Error Models

In order to assess the impact of the nominal error models on the availability achieved by the baro-augmented ARAIM algorithm world-wide, 72 simulations were run with different values of nominal bias and uncertainty of the geodetic altitude measurement:

- $\sigma_{int,Baro} \in \{7.5, 10, 12.5, 15, 17.5, 20, 30, 50, 75, 100, 150, 200\}$ m ,

- $b_{nom,Baro} \in \{0, 0.5, 1, 1.5, 2, 2.5\}$ m .

The accuracy model is obtained with $\sigma_{acc,Baro} = (\frac{2}{3})\sigma_{int,Baro}$. This mimics the relationship between the σ_{acc} and σ_{int} for both GPS and Galileo (Working Group C, 2016).

Figure 6 provides the results of these simulations, together with the ones of the baseline ARAIM. In particular, it shows the world coverage of the LPV-200 service's 99.5% availability as a function of $\sigma_{int,Baro}$ and $b_{nom,Baro}$. It can be seen that even when $\sigma_{int,Baro}$ takes relatively large values, the availability achieved with the baro-augmented ARAIM is slightly higher than the one achieved with the baseline ARAIM, i.e. 98.37%, which is represented by the grey surface. In particular, the coverage achieved with the baro-augmentation was found to be 100% even for $\sigma_{int,Baro} = 100$ m and for each of the tested $b_{nom,Baro}$ values.

The influence of the $b_{nom,Baro}$ on the availability coverage for the given requirements was found to relatively mild. However, as expected, it was found that the higher was the value of $b_{nom,Baro}$, the lower was the availability coverage. This can be seen from the aforementioned Figure especially for the higher $\sigma_{int,Baro}$. In particular, for $\sigma_{int,Baro} = 200$ m, the coverage was found to be of 99.08% for $b_{nom,Baro} = 0$ m and 98.87% for $b_{nom,Baro} = 2.5$ m.

Figure 7 is analogous to Figure 6, whereby the VAL is decreased from 35 to 20 m, that is the VAL adopted for the APV-II (ICAO, 2006a). This allows to better understand the performance improvement in terms of availability that is introduced by the baro-augmentation. Furthermore, it also allows to better assess the influence of the nominal error models on the availability
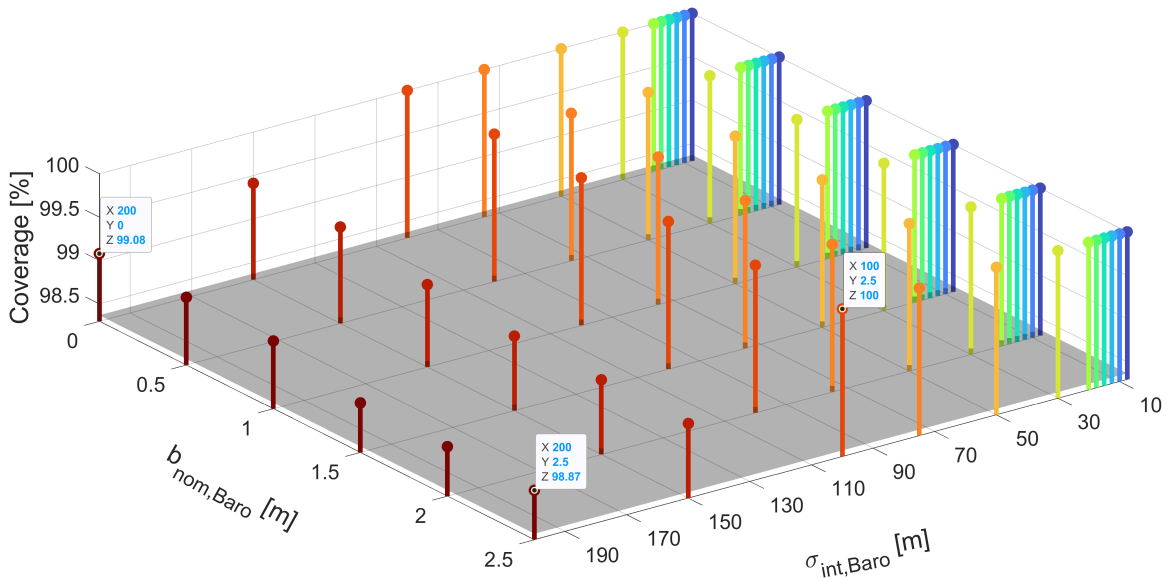
Figure 6: World surface coverage of the LPV-200 (with VAL = 35 m.) availability's 99.5 percentile as a function of $\sigma_{int,Baro}$ and $b_{nom,Baro}$. The grey surface represents the baseline ARAIM coverage level.
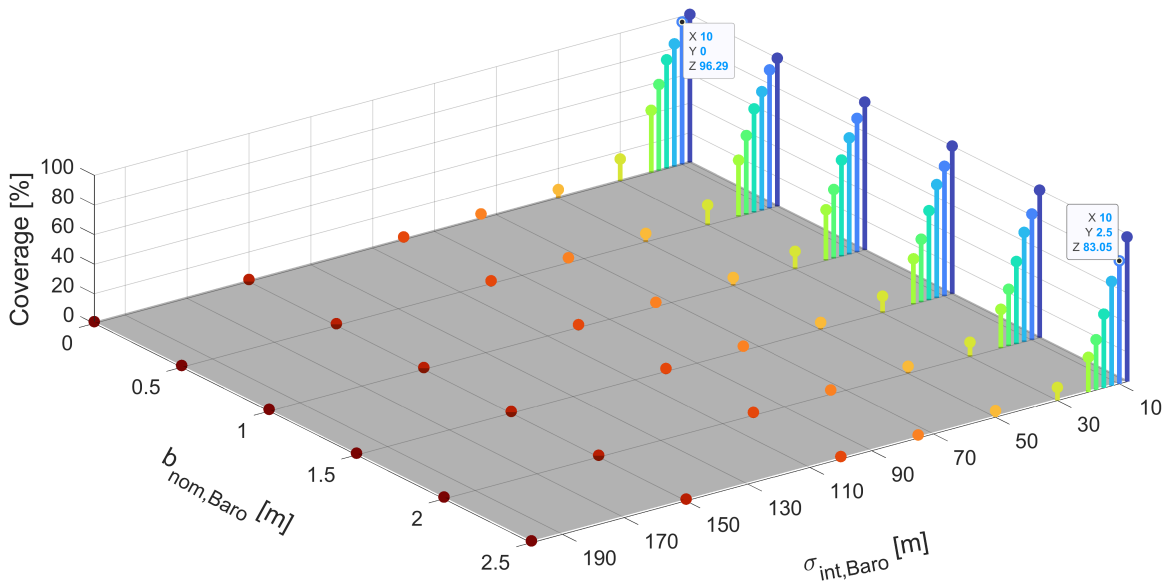

Figure 7: World surface coverage with VAL = 20 m availability's 99.5 percentile as a function of $\sigma_{int,Baro}$ and $b_{nom,Baro}$. The grey surface represents the baseline ARAIM coverage level.

coverage.

The influence of $b_{nom,Baro}$ can in this case be seen from this Figure by looking in particular at the lower $\sigma_{int,Baro}$ values. In particular, for $\sigma_{int,Baro} = 10$ m, the coverage was found to be of 96.3% for $b_{nom,Baro} = 0$ m and 83% for $b_{nom,Baro} = 2.5$ m. As for the case with VAL = 35 m, already for $\sigma_{int,Baro} = 100$ m, the baro-augmented ARAIM slightly outperforms the baseline ARAIM, which reaches a coverage of 1.2% only. Furthermore, the baro-augmented ARAIM was found to achieve a coverage of 100% by for $\sigma_{int,Baro} = 7.5$ m and for $b_{nom,Baro} \leq 1$ m. This can be seen in Figure 8, for $b_{nom,Baro} = 1$ m.
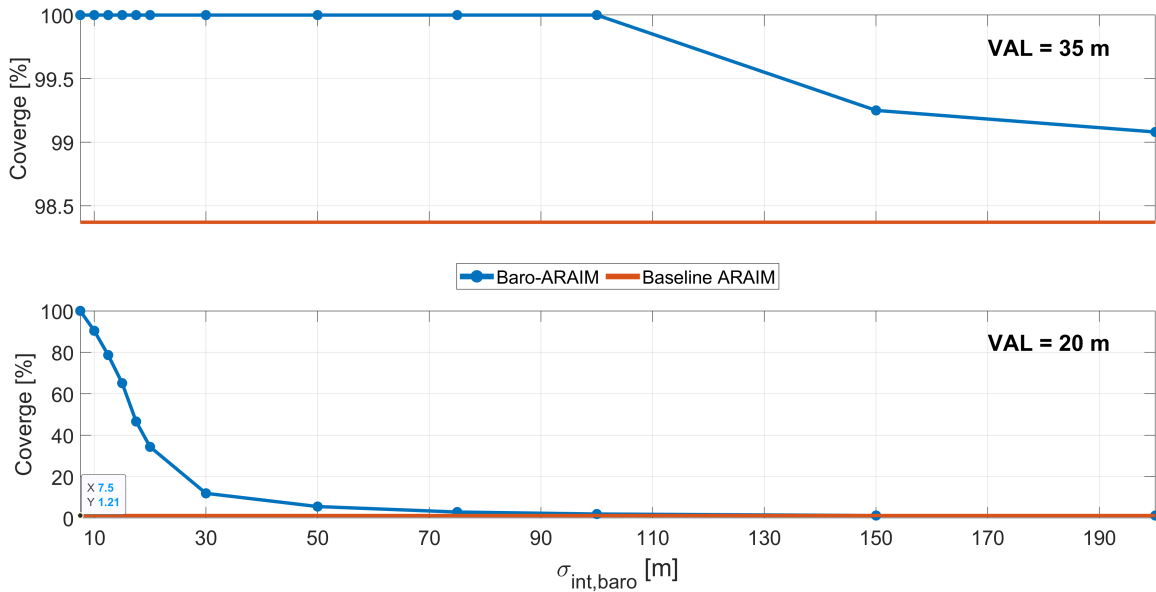
Figure 8: World surface coverage of the LPV-200 availability's 99.5 percentile, with different VALs, as a function of $\sigma_{int,Baro}$, with $b_{nom,Baro} = 1$ m

2. Availability Simulations with flight Data Nominal Error Models

An availability simulation of the baro-augmented ARAIM was run by using the nominal error models presented in Subsection III.1. For this run, the world grid was refined by setting $\Delta L = 5$ deg. and $\Delta \lambda = 5$ deg.. A simulation of the baseline ARAIM was run on this refined world grid too, for comparing the results of the baro-augmented ARAIM to the ones of the baseline ARAIM.
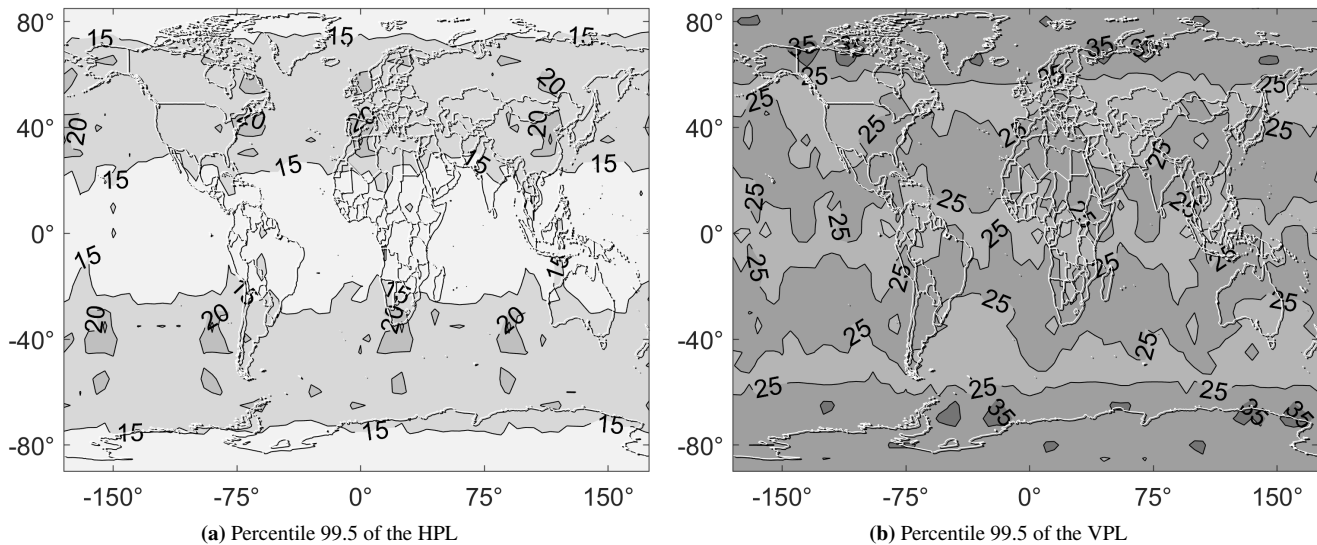

(a) Percentile 99.5 of the HPL

(b) Percentile 99.5 of the VPL

Figure 9: Protection levels results of the baseline ARAIM applied to the simulation, over one day

Figure 9 and Figure 10 show the results of the baseline and of the baro-augmented, respectively. By comparing the two aforementioned figures, it can be seen that the baro-augmentation is able to relatively greatly reduce the VPLs worldwide. The reduction in the HPLs is comparably negligible instead.
Figure 11a and Figure 11b show the percentile 99.5 of the LPV-200 availability achieved with the baseline ARAIM and the one attained with the baro-augmented ARAIM, respectively. By comparing the two, it can be noticed that the baro-augmentation
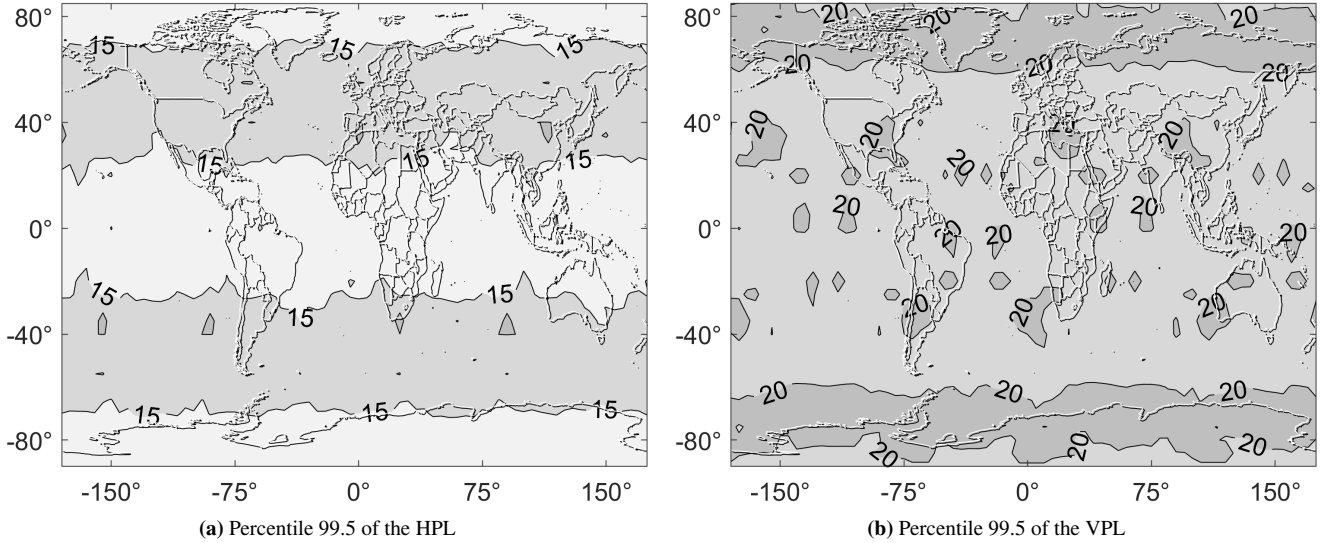
(a) Percentile 99.5 of the HPL

(b) Percentile 99.5 of the VPL

Figure 10: Protection levels results of the baro-augmented ARAIM applied to the simulation, over one day

extends the LPV-200 availability in the simulation to 100% worldwide. The baseline ARAIM achieves a 98.6% surface coverage of the 99.5% availability, instead. Furthermore, it was found that the baro-augmented ARAIM achieves an availability coverage of approximately 63%, when the VAL is decreased form 35 to 20 m.
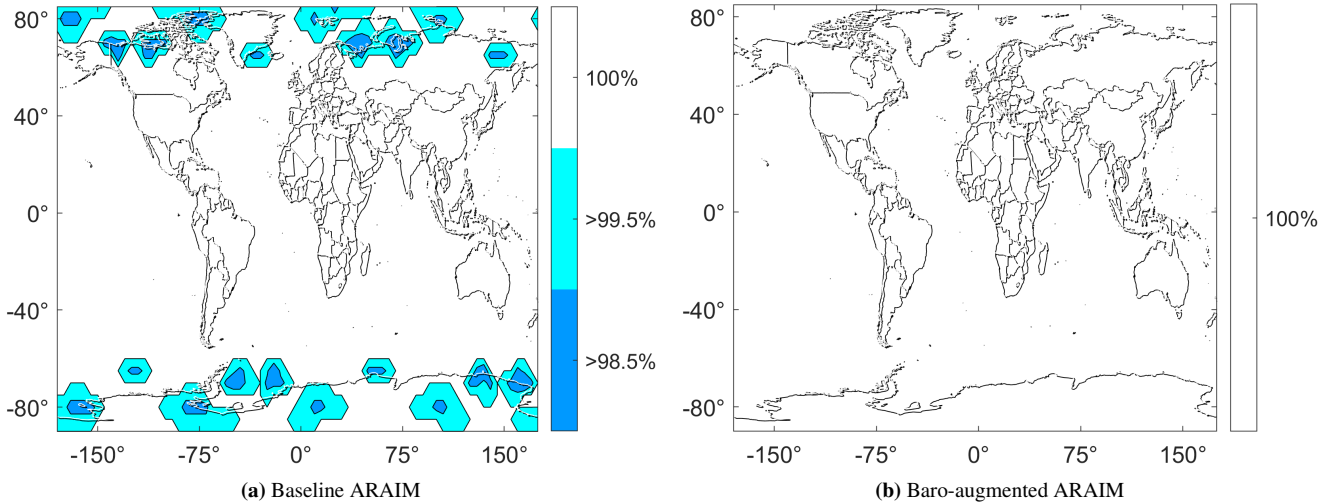

(a) Baseline ARAIM

(b) Baro-augmented ARAIM

Figure 11: LPV-200 Availability over one simulation day

V. FLIGHT DATA EVALUATION

The GNSS/Barometer integration algorithm shown in Figure 1 was evaluated with real flight data gathered during a test flight performed in July 2018 with DLR's Dassault Falcon 20-ES aircraft. The three-dimensional trajectory of this flight is shown in Figure 12a. The GNSS parameters required for ARAIM (baseline and baro-augmented) that were used in this evaluation were the same employed within the simulations described in Section IV, with the exception of the following parameters:

- $\sigma_{URA,GPS,i} = 2.4$ m, $\quad \sigma_{URE,GPS,i} = 2/3 \times 2.4$ m $\quad$ for $i = 1...n_{GPS}$,

- $\sigma_{URA,Gal,i} = 2.4$ m, $\quad \sigma_{URE,Gal,i} = 2/3 \times 2.4$ m $\quad$ for $i = 1...n_{Gal}$.

These modifications were performed because these values, that are mentioned in (Working Group C, 2016), were considered to

be more realistic for the specific GNSS measurements that were used for this assessment and for the time when the flight was carried out.

The values assigned to the additional constants and parameters mentioned in II are the ones recommended for LPV-200 (Working Group C, 2016).

The GNSS code and phase measurements that were employed were in the following frequencies:

- GPS: L1 & L2 ,
- Galileo: E1 & E5b .

This choice was taken because the number of available GNSS measurements at the time of the flight was remarkably higher in the employed frequencies rather than in the frequencies specified by ARAIM standards (Working Group C, 2016), that are L1 & L5 for GPS and E1 & E5a for Galileo. Compared to the availability simulations, the flight data evaluation captures the evolution of visible satellites due to the aircraft manoeuvres. At the time of the flights, it is important to note that the Galileo constellation was not complete. For the processing of the data a cycle-slip detector was also considered. This reduces in some cases the availability of satellites since smoothing filters need time to re-initialize.
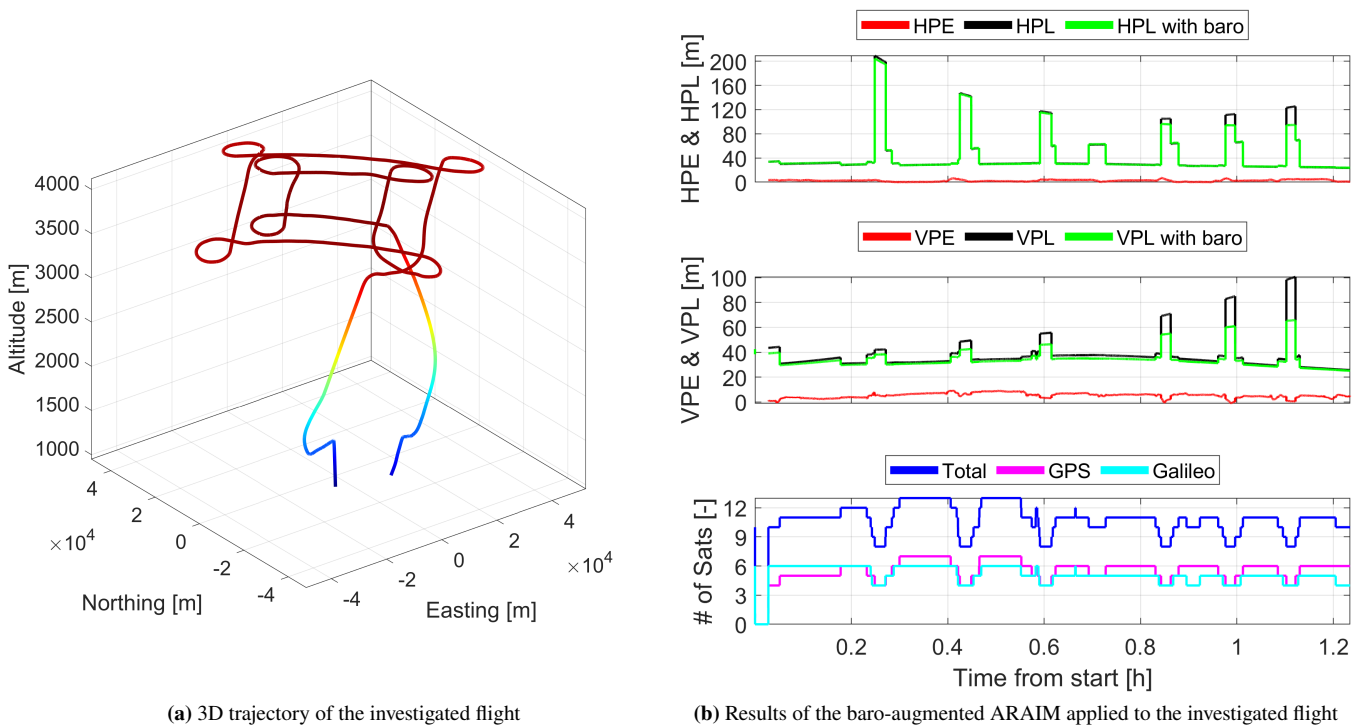

(a) 3D trajectory of the investigated flight

(b) Results of the baro-augmented ARAIM applied to the investigated flight

Figure 12: Baro-augmented ARAIM application to a real flight

The upper plot in Figure 12b shows the Horizontal Position Error (HPE) and the HPL achieved with the baro-augmented ARAIM along the trajectory, as well as the HPL achieved with the baseline ARAIM. The HPE achieved without the baro-augmentation is not shown, because the changes in the HPE introduced by the baro-augmentation were found to be almost negligible.

As can be seen from this plot, the two HPLs are approximately the same outside of those flight phases when the sharper maneuvers were flown. During some of these phases, and in particular in the three last ones, the baro-augmentation was able to reduce the HPL by up to 30 m, approximately.

The central plot in Figure 12b shows the Vertical Position Error (VPE) and the VPL achieved with the baro-augmented ARAIM along the trajectory. It shows the VPL achieved with the baseline ARAIM, too. As for the horizontal domain, the changes in the position error due to the baro-augmentation were found to be almost negligible. For this reason, the VPE without the baro-augmentation is not shown.

In a counterintuitive way, the VPE decreases during the intervals when less satellite measurements are available. A potential reason for this, is that the measurements from one or more faulted satellites or one or more satellites at considerably low elevation angle(s) was or were excluded from the all-in-view solution computation. This behavior can partially be seen in the development of the HPE as well.

As it can be seen from this plot, the baro-augmented ARAIM outperforms the baseline ARAIM in terms of the VPL along

the whole flight. In particular, outside of the sharper maneuvers, the VPL is reduced by approximately up to 3 m. During the maneuvers, the reduction in the VPL reached almost 35 m, instead.

The baro-augmented ARAIM is therefore able to reduce the protection levels, especially in cases of reduced reception of satellite measurements.

VI. CONCLUSIONS AND FUTURE WORK

This work supports the inclusion of airborne barometric pressure measurements, aided by external weather data, into a safe GNSS autonomous integrity architecture following the last developments in ARAIM.

For this purpose, the paper briefly presents the methodology adopted for the computation of geodetic altitude from the pressure measurements and the weather data, which is described in detail within a previous publication of the authors. The paper then describes the derivations of the nominal error models and threat model of this geodetic altitude, which are required for its inclusion into ARAIM. The derivations of the models presented in this work are based on several hours of flight data collected during a flight tests campaign performed in 2018 with the DLR's Dassault Falcon 20-ES aircraft. The altitude span and the horizontal distances covered during these flights allow the barometric pressure measurements to reflect the effects due to changes in weather, flight dynamics, and altitude more than they would in a flight simulator or during static sensors runs. However, further analysis with different aircrafts or sensors and in different times of the year or locations would still be necessary to gain confidence in the error and threat models.

The simulations show that the baro-augmentation is capable of extending the surface coverage of the LPV-200 100% availability world-wide, when employing the derived error models. Even when the VAL is decreased from 35 to 20 m, the simulations show that the baro-augmented ARAIM achieves a 63% world coverage of 99.5% availability, as opposed to the 1.2% coverage attained with the baseline ARAIM. Additionally, further simulations allowed to find that the proposed architecture has the potential of achieving a 100% coverage even with these stricter requirements if tighter, hypothetical, nominal error models are used. This motivates future efforts in the derivation of tighter error models by analyzing data collected during many other flights performed with different kinds of airplanes.

The implementation along the real flight shows that the integration of the barometric geodetic altitude with GNSS may have a marginal impact in the positioning accuracy in normal flight situations. However, the baro-augmentation is found to have a non-negligible impact on the protection levels. Indeed, a comparison of the protection levels achieved with and without the baro-augmentation shows that the HPL and the VPL were decreased by approximately up to 30 and 35 m, respectively during aircraft banking.

The analyses presented in this work rely on external weather data, obtained from weather reanalyis, i.e. estimations of past weather. However, future work will employ weather forecasts in order to enable a real-time implementation of the proposed architecture. Finally, future work will investigate the possibility of applying the baro-augmentation to UAVs. In this case, the barometric geodetic altitude would be obtained from airborne barometric pressure measurements and pressure and temperature measurements performed on the ground. This would require a change in the derivation of the threat model. New error models specific to UAV applications would need to be derived too.

ACKNOWLEDGEMENTS

REFERENCES

Blanch, J., Walter, T., Enge, P., Lee, Y., Pervan, B., Rippl, M., Spletter, A., and Kropp, V. (2015). Baseline Advanced RAIM User Algorithm and Possible Improvements. *IEEE Transactions on Aerospace and Electronic Systems*, 51(1):713–732. DOI: 10.1109/TAES.2014.130739.

Di Vito, V. and Torrano, G. (2017). A Tactical Separation System for Small Air Transport Vehicles. In *7th EASN 2017 International Conference on Innovation in European Aeronautics Research, Warsaw, Poland*. CIRA, Italian Aerospace Research Center and Honeywell International s.r.o .

ECMWF (2020). Fact sheet: Reanalysis. [Online]. Available: `https://www.ecmwf.int/en/about/media-centre/focus/2020/fact-sheet-reanalysis`, Last accessed on Sep 21, 2022.

Gaglione, S., Angrisano, A., Castaldo, G., Gioia, C., Innac, A., Perrotta, L., Core, G. D., and Troisi, S. (2015). GPS/Barometer Augmented Navigation system: Integration and Integrity Monitoring. In *2015 IEEE Metrology for Aerospace (MetroAeroSpace)*.

Garcia Crespillo, O. (2022). GNSS/INS Kalman Filter Integrity Monitoring with Uncertain Time Correlated Error Processes. [Online]. Available: `https://infoscience.epfl.ch/record/292087`, Last accessed on Sep 23, 2022.

Hersbach, H., Bell, B., Berrisford, P., Biavati, G., Horányi, A., Sabater, J. M., Nicolas, J., Peubey, C., Radu, R., Rozum, I., Schepers, D., Simmons, A., Soci, C., Dee, D., and Thépaut, J.-N. (2018). ERA5 hourly data on pressure levels from 1959 to present. DOI: 10.24381/cds.bd0915c6, (Accessed on 2022-09-23).

ICAO (2006a). *Annex 10 to the Convention on International Civil Aviation, Aeronautical Telecommunications, Volume I Radio Navigation Aids*, 6th edition.

ICAO (2006b). *Procedures for Air Navigation Services, Volume I, Flight, Procedures, Doc 8168, OPS/611*.

ICAO (2013). *Performance Based Navigation Manual, Consolidated 4th Edition, Doc 9613*.

Lee, J., Hyeon, E., Kim, M., and Lee, J. (2016). Vertical Position Error Bounding for Integrated GPS/Barometer Sensors to Support Unmanned Aerial Vehicle (UAV). In *30th Congress of the International Council of the Aeronautical Sciences (ICAS)*. DOI: 10.33012/2020.17542.

Lerro, A. and Battipede, M. (2021). Safety Analysis of a Certifiable Air Data System Based on Synthetic Sensors for Flow Angle Estimation. *Applied Sciences*, 11(7):1806–1815. [Online]. Available: `https://www.mdpi.com/2076-3417/11/7/3127`, DOI: 10.3390/app11073127.

Piwek, K. and Wiśniowski, W. (2016). Small air transport aircraft entry requirements evoked by FlightPath 2050. *Aircraft Engineering and Aerospace Technology*, 88(2):341–347.

Quanterion Solutions Incorporated (2016). *Quanterion Nonelectronic Parts Reliability Data—2016*. Reliability Databook Series, Quanterion Solutions Incorporated.

RTCA (2020). *DO-384 Minimum Operational Performance Standards (MOPS) for GNSS Aided Inertial Systems*.

S. Jan, D., Gebre-Egziabher, Walter, T., and Enge, P. (2008). Improving GPS-Based Landing System Performance Using an Empirical Barometric Altimeter Confidence Bound. *IEEE Transactions on Aerospace and Electronic Systems*, 44(1).

Simonetti, M. and Garcia Crespillo, O. (2021). Robust Modeling of Geodetic Altitude from Barometric Altimeter and Weather Data. In *ION GNSS+ 2021 St. Louis*.

SKYbrary (2021). Altitude, Flight Level and Height. [Online]. Available: `https://www.skybrary.aero/index.php/Altitude,_Flight_Level_and_Height`, Last accessed on Sep 23, 2022.

Torens, C., Volkert, A., Becker, D., Gerbeth, D., Schalk, L., Crespillo, O. G., Zhu, C., Stelkens-Kobsch, T., Gehrke, T., Metz, I. C., and Dauer, J. (2021). HorizonUAM: Safety and Security Considerations for Urban Air Mobility. [Online]. Available: `https://arc.aiaa.org/doi/abs/10.2514/6.2021-3199`, DOI: 10.2514/6.2021-3199.

Walter, T. and Blanch, J. (2019). MAAST. [Online]. Available: `https://gps.stanford.edu/resources/software-tools/maast`, Last accessed on Sep 23, 2022.

Walter, T., Blanch, J., Gunning, K., Joerger, M., and Pervan, B. (2019). Determination of Fault Probabilities for ARAIM. *IEEE Transactions on Aerospace and Electronic Systems*, 55(6):3505–3516. DOI:10.1109/TAES.2019.2909727.

Working Group C (2016). GPS-Galileo Working Group C ARAIM Technical Subgroup Milestone 3 Report. Technical report. [Online]. Available: `https://www.gps.gov/policy/cooperation/europe/2016/working-group-c/`, Last accessed on Sep 23, 2022.

Xu, X., Lai, J., Liu, M., Zheng, Z., Dai, Y., and Huang, K. (2021). An Improved Weight Optimization AAIM Method Aided by Barometric. *International Journal of Aeronautical and Space Sciences*, 22(5):638–647.